THE JOURNAL OF PHYSICAL CHEMISTRY A
A JOURNAL OF THE AMERICAN CHEMICAL SOCIETY

pubs.acs.org/JPCA Article

Electron Binding Energy Spectra of Al_nPt^- Clusters—A Combined Experimental and Computational Study

Paulo H. Acioli,* Xinxing Zhang, Kit H. Bowen,* and Julius Jellinek*

Cite This: *J. Phys. Chem. A* 2022, 126, 4241−4247 Read Online

ACCESS | Metrics & More | Article Recommendations | Supporting Information

ABSTRACT: Results of size-selected electron photo-detachment experiments and density functional theory calculations on anionic Al_nPt^-, n = 1−7, clusters are presented and analyzed. The measured and calculated spectra of electron binding energies are, overall, in excellent accord with each other. The analysis reveals the general importance of accounting for the multiplicity of structural forms of a given-size cluster that can contribute to its measured spectrum, especially when the clusters are fluxional and/or the conditions of the experiment allow for structural transitions. We show that for the systems studied here, the size-specific peculiarities of the measured spectra can be understood in terms of the combined contributions of corresponding different accessible stable equilibrium conformations, *bona-fide* transition-state configurations, and electronic-crossing structures that may play the role of effective barriers in electronically nonadiabatic dynamics.

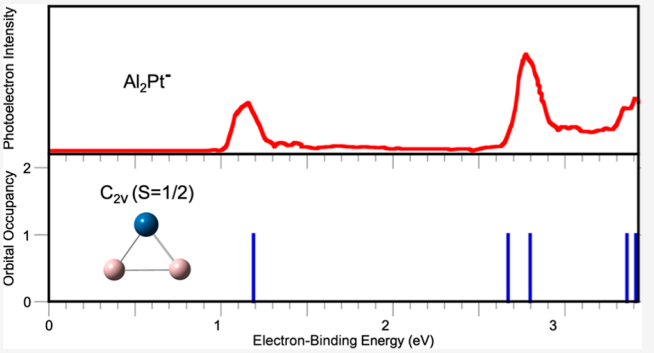

INTRODUCTION

Electron spectroscopy continues to be used as a powerful and versatile tool for the interrogation and characterization of a broad variety of systems, both extended and finite size. Its capabilities are particularly well demonstrated and utilized in the realm of atomic clusters and nanosystems—a field that is characterized by an extraordinary richness of properties and features. This richness arises from an intricate interplay between the simultaneous, and, in general, coupled effects of size and composition. The various characteristics, including the spectra of electron binding energies (EBEs), depend sensitively on the size, composition (both elemental and percentile), and structure(s) of the systems; the structures themselves are functions of the preceding two factors and, in the case of small-size systems, they also may depend on the charge state.

Experimental information on EBE spectra is usually obtained through photodetachment measurements on size-selected clusters (see, *e.g.*, refs 1 and 2 and the citations therein). The measured spectra contain detailed information on the systems studied, but this information is encoded in terms of the cumulative effects of the different factors mentioned above. In order to decode this information into and correlate it with the individual characteristics of a system, for example its structure(s), one needs to complement the measured spectra with results of high-accuracy calculations. Such results are furnished by what can be referred to as *computational electron spectroscopy* (see, *e.g.*, ref 3 and the citations therein). The latter plays a central role in furnishing an interpretation of the individual features in measured spectra and in providing an overall, fundamental level of understanding. A number of factors may contribute to such an understanding. One of these is the possible contribution of multiple stable structural forms of the studied system. These structural forms may be in the same or different electronic states.[4] Moreover, transient unstable structures involved in the possible interconversions of the stable structures under the conditions of the experiment may contribute to the measured data as well. Identifying all these and their contributions to an experimental EBE spectrum is an integral task of the computational component of the studies.

Another important task of computational electron spectroscopy is to try to identify the separate roles of size, composition, and structure in evolving the EBE spectrum of one system (the "parent"—*e.g.*, a single-component cluster) into that of another system (the "daughter"—*e.g.*, a two-component cluster).[4,5] An advancement in understanding these roles and the trends associated with them will greatly expand our conceptual framework. But it also will have a major practical/technological impact on our ability to formulate design and synthesis

Received: May 5, 2022
Revised: June 6, 2022
Published: June 24, 2022

https://doi.org/10.1021/acs.jpca.2c03116
J. Phys. Chem. A 2022, 126, 4241−4247

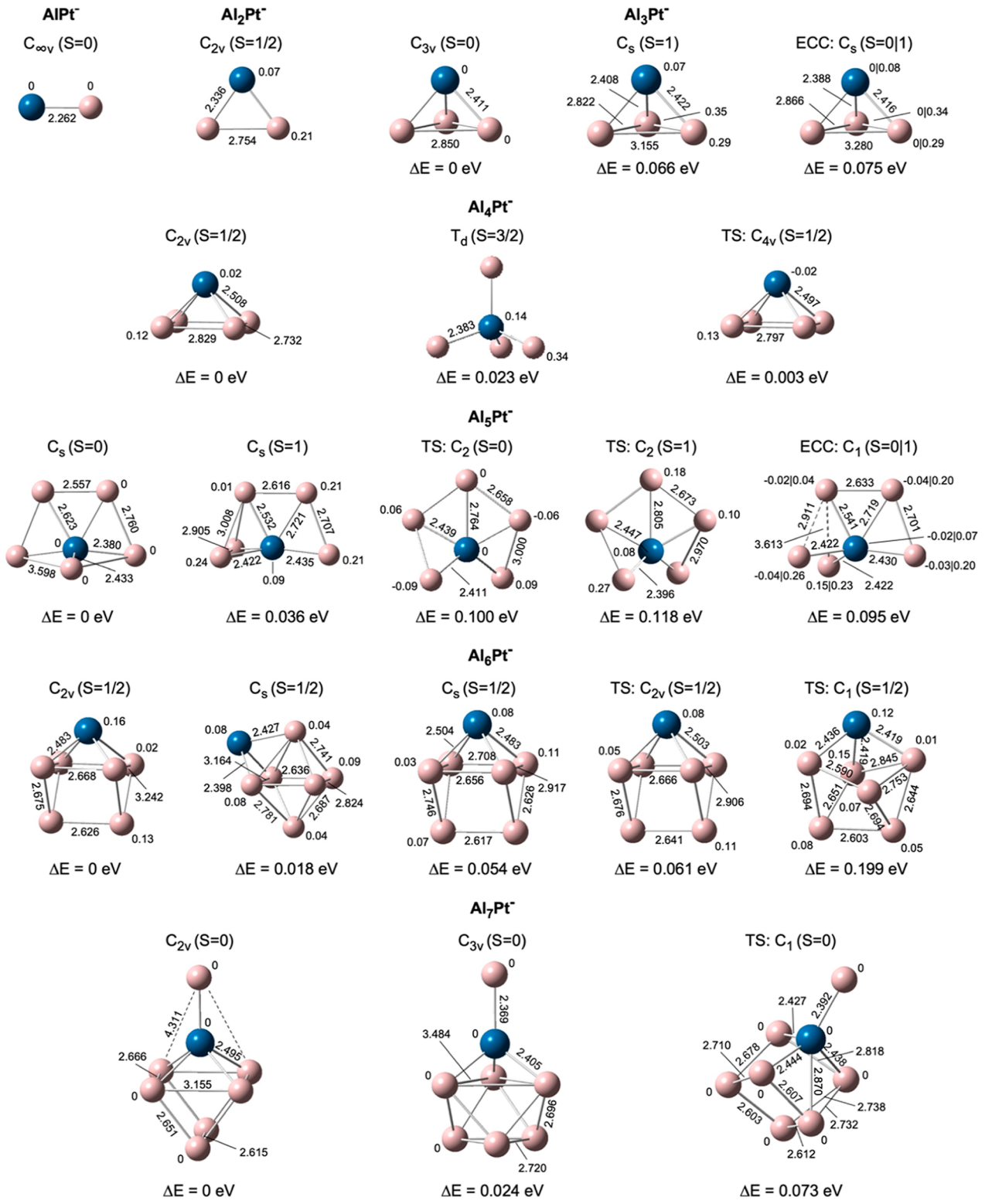

Figure 1. Low-energy structures of Al_nPt^-, n = 1−7, clusters identified in our calculations and their characteristics, which include their total energy ΔE (in eV) referred to the energy of the corresponding most stable conformation, point group symmetry, total spin (S), atomic spins, and interatomic distances (in Å). The Al atoms are tan and the Pt atom is blue.

schedules that will produce finite-size systems with properties and functionalities finely tuned to desired specifications.

Here, we continue our combined experimental/computational explorations of one-component and bimetallic metal clusters[4−11] by presenting a thorough analysis of the EBE spectra of Al_nPt^-, n = 1−7, systems. Our focus on metal clusters is motivated by their technological relevance. In the next section, we outline the experimental and theoretical/computational details. The results are then presented and discussed in the following section. A brief summary is given in the conclusion.

https://doi.org/10.1021/acs.jpca.2c03116
J. Phys. Chem. A 2022, 126, 4241−4247

METHODOLOGICAL DETAILS

Experimental Section. Our photoelectron spectroscopy (PES) apparatus consists of a pulsed arc cluster ionization source (PACIS), a time-of-flight mass spectrometer, a Nd:YAG photodetachment laser, and a magnetic bottle electron energy analyzer with a resolution of ~35 meV at 1 eV electron kinetic energy (EKE); the details can be found in refs 12 and 13. The known atomic transitions in Cu^-[14] were used for calibration of the photoelectron spectra.

The Al_nPt^- cluster ions were generated in the PACIS. In this source, a strong current is discharged through a sample, which in our case was a mixture of aluminum and platinum powders pressed onto an Al rod. The carrier gas was helium, which was supplied by a pulsed gas valve behind the discharge region. The carrier gas cools down the initially hot clusters, but their temperature is difficult to evaluate. We roughly estimate it to be ~150 K above room temperature.

The PES measurements were performed by crossing a beam of mass-selected Al_nPt^- with a fixed-frequency photon beam and energy-analyzing the photodetached electrons. The photon energy was 3.49 eV. The EBEs were obtained from the energy balance equation

$$\mathrm{EBE} = h\nu - \mathrm{EKE} \quad (1)$$

where h is Planck's constant and ν is the photon frequency.

Theoretical/Computational Framework. The framework of the gradient-corrected density functional theory (DFT) was used to determine the low-energy structural forms of the Al_nPt^-, n = 1−7, clusters. The calculations were performed with the Becke exchange[15] and Perdew correlation[16] functionals (BP86). The Stuttgart pseudopotential for Pt with a (8, 7, 6|6, 5, 3) basis set for the remaining 18 electrons[17] and an all-electron treatment for Al with a DGZTVP basis set,[18,19] as implemented in the Gaussian-03 package,[20] were utilized. This selection of the computational framework was based on test calculations that included a number of alternative choices and were performed on Al and Pt atoms and their diatomic molecules (see the Supporting Information for details).

Many initial guess structures—isomeric and homotopic (the latter correspond to different possible placements of the Pt atom within a chosen isomeric form[21])—and different spin states were considered for each cluster size. These structures were then fully optimized using gradient-based techniques with no symmetry constraints imposed; the convergence criteria for the configurational energy and the displacement were 10^{-6} H and 4×10^{-6} Å, respectively. Normal mode analysis was applied to the resulting equilibrium structures to confirm that they correspond to stable equilibria. In addition, we also performed searches for transition state (TS) configurations. These were carried out using constrained energy minimizations on a grid of fixed distances that converted the interatomic separation between a chosen pair of atoms in one stable equilibrium configuration into that in another equilibrium configuration. We also explored possible transitions between two stable equilibrium conformations in different electronic states (*i.e.*, with different spins). The configurations corresponding to the crossing (degeneracy) of such different electronic states—the electronic crossing configurations (ECCs)—were obtained through constrained energy minimizations performed on two grids of fixed distances originating from the interatomic separations between the same chosen pair of atoms in the two equilibrium configurations involved. The constrained minimizations on each grid were carried out keeping the corresponding electronic state (*i.e.*, spin) fixed. The grids were followed in the directions that caused the energies of the two structures to advance toward each other (see the Supporting Information for details). All the calculations were carried out using the unrestricted formalism.

The calculated EBE spectra were obtained by converting the (nonphysical) Kohn−Sham (KS) eigenenergies of the clusters, as furnished by the DFT calculations, into binding energies of the corresponding electrons. This was accomplished using a correction scheme we developed earlier.[22] The scheme is rigorous in that it uses only ground-state properties obtained *via* traditional (*i.e.*, time-independent) DFT calculations, it yields orbital-specific corrections, and it has been shown to provide highly accurate results.[4−11,23] Specifically, for each i-th KS eigenenergy ϵ_i, the scheme furnishes a correction term Δ_i such that the EBE_i of the corresponding electron is defined by the equation

$$\mathrm{EBE}_i = -\epsilon_i + \Delta_i \quad (2)$$

RESULTS AND DISCUSSION

Structural and Energetic Characteristics. The low-energy stable equilibrium structures we identified for Al_nPt^-, n = 1−7, are shown together with their characteristics in Figure 1. The figure also shows, when found, the low-energy unstable equilibrium TS conformations and the nonequilibrium ECCs that serve as bridges between the stable equilibrium structures.

A common motif of the most stable conformations for all sizes is that the Pt atom occupies a site with high coordination to Al atoms. The Pt−Al neighbor distances in these conformations range from 2.262 to 2.623 Å and are shorter than the Al−Al neighbor distances that vary from 2.557 to 3.598 Å. The spin states of these conformations are all singlets for clusters with an odd number of Al atoms and doublets for cluster with an even number of Al atoms.

For Al_2Pt^-, we have a single configuration. For Al_3Pt^-, there are three conformational structures. Two of these, $C_{3v}(S = 0)$ and $C_s(S = 1)$, represent stable equilibria, and the third is a $C_s(S = 0|S = 1)$ ECC for which the spin $S = 0$ and $S = 1$ electronic states are degenerate and which serves as an effective dynamical barrier between the $C_{3v}(S = 0)$ and $C_s(S = 1)$ structures. Three conformations are also identified for Al_4Pt^-. Two of these, $C_{2v}(S = 1/2)$ and $T_d(S = 3/2)$, are stable equilibria, and the third, $C_{4v}(S = 1/2)$, is a TS configuration that connects the $C_{2v}(S = 1/2)$ structure with its permutational equivalent. The case of Al_5Pt^- presents five structures. Two of these, $C_s(S = 0)$ and $C_s(S = 1)$, are stable equilibrium configurations; the other two, $C_2(S = 0)$ and $C_2(S = 1)$, are TSs that connect, respectively, the $C_s(S = 0)$ and the $C_s(S = 1)$ equilibria with their corresponding permutational equivalents; and the fifth, $C_1(S = 0|S = 1)$, is an ECC that serves as an effective dynamical barrier between the $C_s(S = 0)$ and $C_s(S = 1)$ structures. Al_6Pt^- also is represented by five configurations. The first three, $C_{2v}(S = 1/2)$, $C_s(S = 1/2)$, and $C_s(S = 1/2)$, are stable equilibrium structures. The other two, $C_{2v}(S = 1/2)$ and $C_1(S = 1/2)$, are TSs. The $C_{2v}(S = 1/2)$ TS connects the second of the two $C_s(S = 1/2)$ stable equilibrium structures with its permutational analogue. The $C_1(S = 1/2)$ TS links the two $C_s(S = 1/2)$ equilibrium structures. Finally, the case of Al_7Pt^- is represented by three structures, two of which, $C_{2v}(S = 0)$ and $C_{3v}(S = 0)$, are stable equilibria, and the third, $C_1(S =$

https://doi.org/10.1021/acs.jpca.2c03116
J. Phys. Chem. A 2022, 126, 4241−4247

0), is a TS configuration that connects the $C_{2v}(S = 0)$ and $C_{3v}(S = 0)$ conformations.

Further examination of Figure 1 indicates that, for each size, all the configurations shown in Figure 1 are well within the room-temperature vibrational energy gap from the corresponding most stable conformation. In addition, the TSs and the ECCs are just a bit higher in energy than the stable equilibrium structures they connect. Consequently, the zero-point energies of these structures may be sufficient to overcome the TSs and the ECCs even when the zero-point energies of the latter are also taken into account. This renders the equilibrium structures fluxional; a very small amount of extra thermal energy will only further enhance the degree of their fluxionality.

Measured and Calculated EBE Spectra. The measured and calculated EBE spectra are shown in Figures 2−8 with the values of the individual EBEs of the most stable structures (and the details of how they were calculated) listed in Table 1.

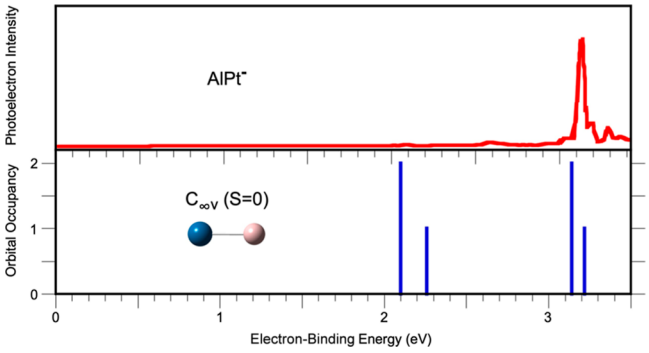

Figure 2. Measured (red continuous line) and calculated (vertical blue lines) EBE spectra of $AlPt^-$.

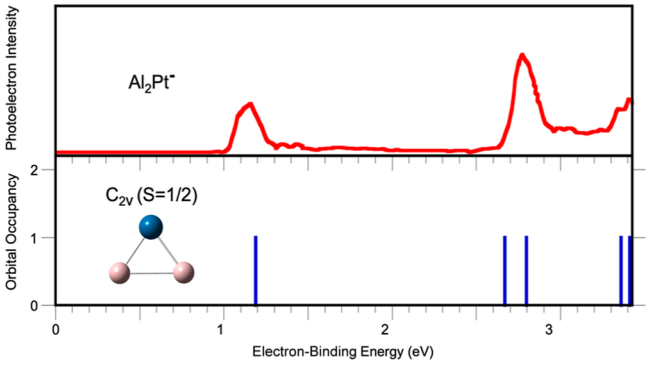

Figure 3. Same as Figure 2, but for Al_2Pt^-.

The results for the $AlPt^-$ dimer are displayed in Figure 2. The puzzling peculiarity of this case is that, whereas the two calculated higher energy EBEs fall remarkably accurately under the peaks of the measured spectrum, the two lower energy ones are hardly represented in the measured data. Essentially, the same finding was obtained in an earlier study[24] that was limited to the cases of $AlPt^-$ and Al_2Pt^-; our calculated EBEs are in good agreement with those of ref 24.

The results for the case of Al_2Pt^- are displayed in Figure 3. Here, the EBEs calculated for the lowest energy structure of the cluster are in remarkably good agreement with the measured spectrum, and this structure alone fully accounts for all the features of the spectrum. That is certainly not the

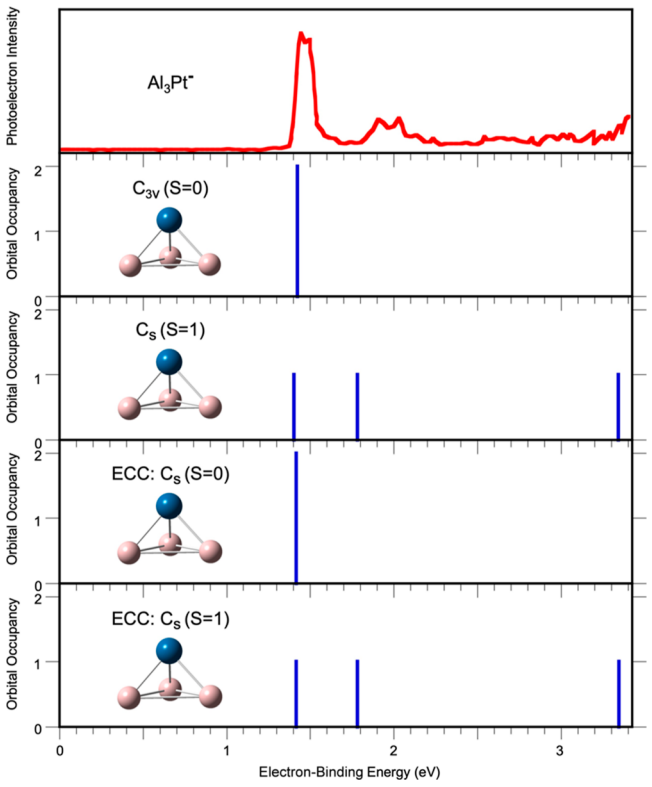

Figure 4. Same as Figure 2, but for Al_3Pt^-. Multiple structures of the cluster contribute to the measured spectrum. See the text for details.

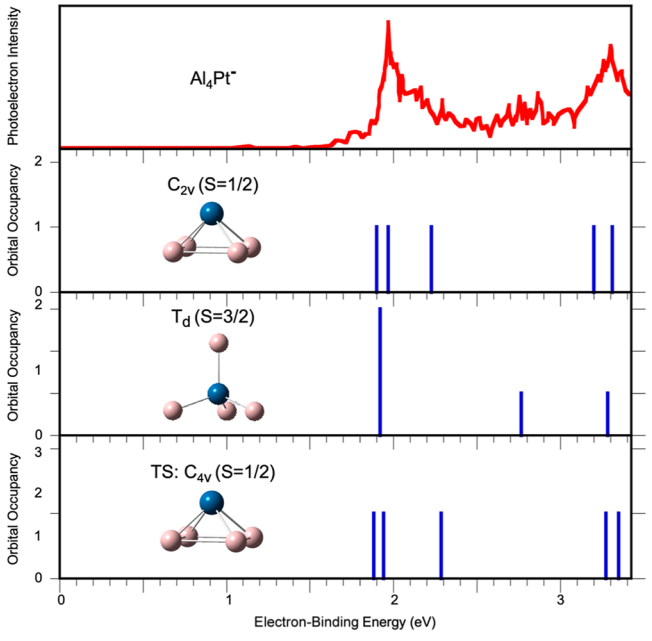

Figure 5. Same as Figure 4, but for Al_4Pt^-.

case for Al_3Pt^- (see Figure 4). Although the calculated EBE of the most stable $C_{3v}(S = 0)$ conformation of this cluster in the relevant energy range falls accurately under the most prominent low-energy peak in the measured spectrum, this conformation alone does not account for the higher-energy spectral features. As is clear from Figure 4, these latter features can be attributed to the contributions of higher energy structures that include the $C_s(S = 1)$ stable equilibrium

https://doi.org/10.1021/acs.jpca.2c03116
J. Phys. Chem. A 2022, 126, 4241−4247

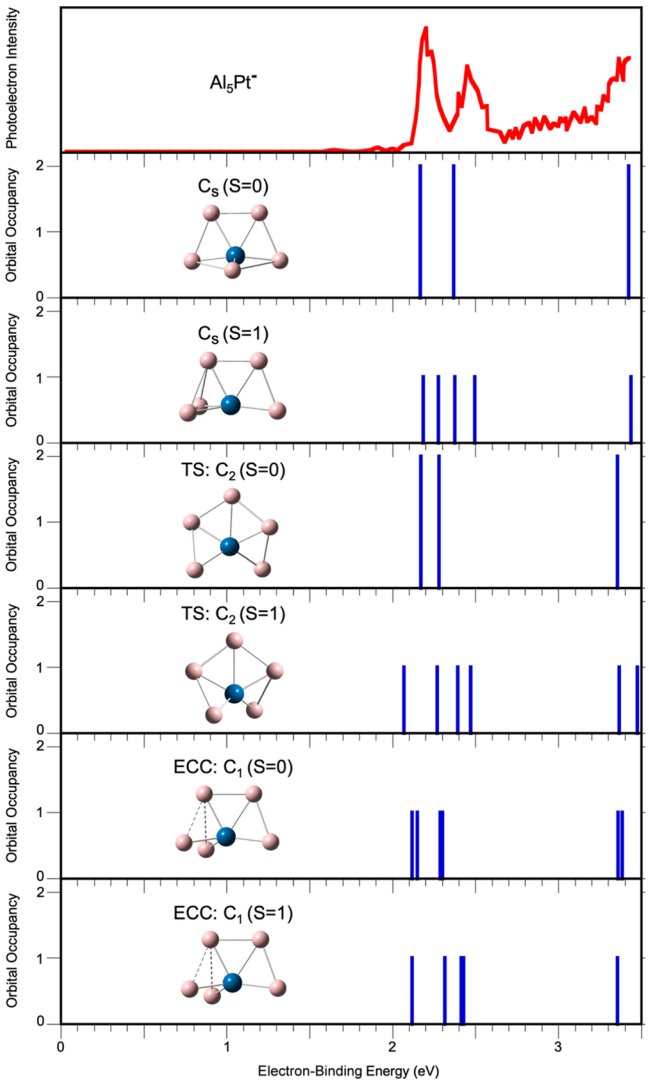

Figure 6. Same as Figures 4 and 5, but for Al_5Pt^-.

conformation, and the $C_s(S = 0)$ and $C_s(S = 1)$ ECCs. Interestingly, the latter three also contribute to the low-energy peak in the measured spectrum, which explains its distinct prominence. The case of Al_4Pt^- is shown in Figure 5. The three structures we identified as contributing to the measured spectrum of this cluster include its most stable $C_{2v}(S = 1/2)$ conformation, its higher energy $T_d(S = 3/2)$ form, and its $C_{4v}(S = 1/2)$ TS configuration. All three contribute to the prominent low-energy and high-energy peaks in the measured spectrum, whereas the less prominent middle peak can be attributed primarily to the $T_d(S = 3/2)$ conformation.

Figure 6 shows our results for Al_5Pt^-. The measured spectrum displays three distinct peaks—two at a low energy and one at a high energy. Our calculations identified six structures that can be viewed as underpinning this spectrum. Two of these are the $C_s(S = 0)$ and $C_s(S = 1)$ stable equilibria, another two are the $C_2(S = 0)$ and $C_2(S = 1)$ TS configurations, and the remaining two are the $C_1(S = 0)$ and $C_1(S = 1)$ ECCs. Examination of the calculated EBEs points to two observations. The first is that the most stable $C_s(S = 0)$ conformation of the cluster alone already accounts for all the major features of the measured spectrum as its calculated EBEs fall ideally under the three prominent peaks. The second

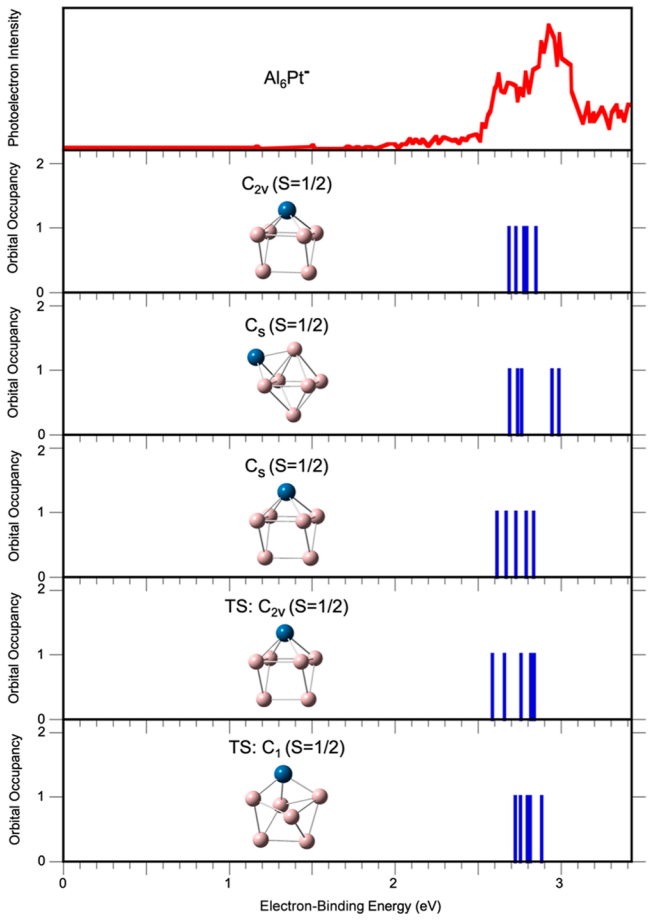

Figure 7. Same as Figure 5, but for Al_6Pt^-.

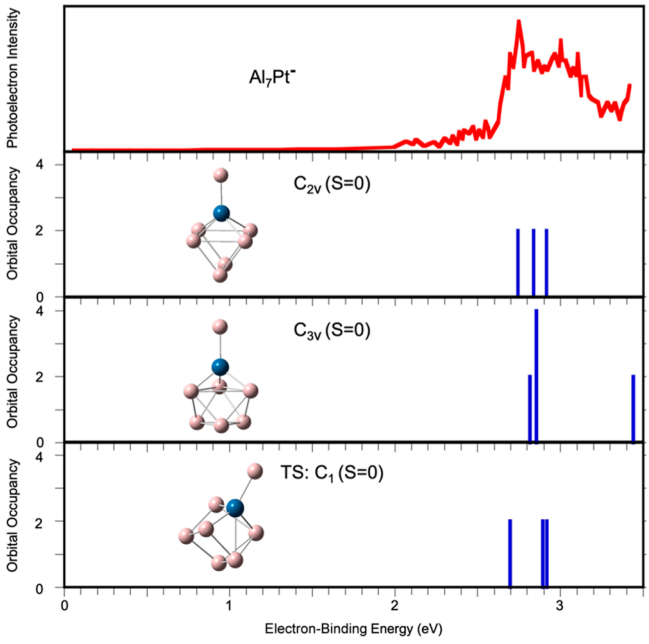

Figure 8. Same as Figure 5, but for Al_7Pt^-.

observation is that the EBEs of all six structures display a similar pattern—they form a low-energy group and a high-energy group of lines. As a consequence, all six can be expected to contribute to each of the three peaks in the experimental spectrum.

https://doi.org/10.1021/acs.jpca.2c03116
J. Phys. Chem. A 2022, 126, 4241−4247

Table 1. Negatives of the Upper Kohn–Sham Eigenenergies ($-\epsilon_i$) and Their Corresponding Correction Terms (Δ_i) and EBE$_i$s for the Lowest Energy Structures of the Al$_n$Pt$^-$, n = 1–7, Clusters[a]

cluster	i	eigenstate label and occupancy	$-\epsilon_i$	Δ_i	EBE$_i$
AlPt$^-$	1	$\boldsymbol{\delta^4}$	**−0.424**	**2.521**	**2.098**
	2	$\boldsymbol{\sigma^2}$	**−0.276**	**2.534**	**2.258**
	3	$\boldsymbol{\sigma^2}$	**0.536**	**2.603**	**3.139**
	4	$\boldsymbol{\pi^4}$	**0.608**	**2.609**	**3.217**
	5	σ^2	3.678	2.861	6.539
Al$_2$Pt$^-$	1	$\mathbf{b_1{}^1(\alpha)}$	**−0.874**	**2.064**	**1.190**
	2	$\mathbf{a_1{}^1(\beta)}$	**0.505**	**2.165**	**2.670**
	3	$\mathbf{a_1{}^1(\alpha)}$	**0.625**	**2.174**	**2.798**
	4	$\mathbf{b_2{}^1(\beta)}$	**1.150**	**2.210**	**3.360**
	5	$\mathbf{a_1{}^1(\beta)}$	**1.199**	**2.213**	**3.412**
	6	$a_2{}^1(\beta)$	1.231	2.215	3.445
	7	$b_2{}^1(\alpha)$	1.267	2.217	3.485
Al$_3$Pt$^-$	1	$\mathbf{a_1{}^2}$	**−0.408**	**1.832**	**1.424**
	2	$a_1{}^2$	1.734	1.976	3.710
Al$_4$Pt$^-$	1	$\mathbf{a_1(\beta)^1}$	**0.052**	**1.849**	**1.901**
	2	$\mathbf{a_1(\alpha)^1}$	**0.117**	**1.851**	**1.968**
	3	$\mathbf{a_1(\alpha)^1}$	**0.366**	**1.862**	**2.228**
	4	$\mathbf{a_2(\beta)^1}$	**1.300**	**1.903**	**3.202**
	5	$\mathbf{a_2(\alpha)^1}$	**1.403**	**1.907**	**3.310**
	6	$b_2(\beta)^1$	1.942	1.931	3.873
Al$_5$Pt$^-$	1	$\mathbf{a'^2}$	**0.391**	**1.778**	**2.168**
	2	$\mathbf{a'^2}$	**0.582**	**1.785**	**2.367**
	3	$\mathbf{a''^2}$	**1.602**	**1.820**	**3.422**
	4	a'^2	1.794	1.826	3.620
Al$_6$Pt$^-$	1	$\mathbf{a_1(\beta)^1}$	**0.818**	**1.867**	**2.685**
	2	$\mathbf{a_1(\alpha)^1}$	**0.858**	**1.868**	**2.726**
	3	$\mathbf{b_1(\beta)^1}$	**0.906**	**1.870**	**2.776**
	4	$\mathbf{a_1(\alpha)^1}$	**0.924**	**1.870**	**2.794**
	5	$\mathbf{b_1(\alpha)^1}$	**0.978**	**1.872**	**2.850**
	6	$b_2(\beta)^1$	1.646	1.889	3.535
	7	$a_1(\beta)^1$	1.738	1.892	3.630
Al$_7$Pt$^-$	1	$\mathbf{a_1{}^2}$	**1.019**	**1.722**	**2.742**
	2	$\mathbf{a_1{}^2}$	**1.112**	**1.724**	**2.836**
	3	$\mathbf{b_1{}^2}$	**1.188**	**1.726**	**2.914**
	4	$a_1{}^2$	1.875	1.739	3.614

[a]All values are in eV. Bold numbers/letters indicate parts of the calculated spectra whose EBE$_i$s fall within the experimental energy range. The attention of the reader is drawn to the magnitude and significant role of the correction terms Δ_i (see the text for details).

The case of Al$_6$Pt$^-$ is presented in Figure 7. The five structures we identified calculationally as contributing to the measured spectrum of this cluster include the $C_{2v}(S = 1/2)$ and the two $C_s(S = 1/2)$ stable equilibrium conformations and the $C_{2v}(S = 1/2)$ and $C_1(S = 1/2)$ TS configurations. Interestingly, it is the pattern of the EBEs of the second stable equilibrium structure, which is higher in energy only by 0.018 eV than the most stable conformation, that matches the shape of the measured spectrum best. Regarding the high-energy tail of the measured spectrum that appears not to be represented explicitly by the EBEs of the five structures, we note that each of these structures has EBEs that fall just outside of the experimental energy range (*cf.*, *e.g.*, the last two EBEs listed for the most stable conformation of Al$_6$Pt$^-$ in Table 1). Upon broadening, these EBEs will contribute to the tail part of the spectrum. In addition, higher energy configurations of the cluster that could be accessible under the conditions of our experiment may contribute to it as well. Finally, the results for Al$_7$Pt$^-$ are shown in Figure 8. The overall broad shape of the spectrum measured for this cluster is well accounted for by the combined pattern of the calculated EBEs of three structures, two of which, $C_{2v}(S = 0)$ and $C_{3v}(S = 0)$, are stable equilibria and the third, $C_1(S = 0)$, is a TS configuration.

The above results and analysis underscore the importance of taking into account the multiplicity of structural forms of a cluster that may contribute to its measured PES spectrum. This is even more true for two-component systems than their one-component counterparts because the extents of the configuration spaces of the former are considerably broader than those of the latter. In addition to the various stable equilibrium conformations, one has also to take into account the possible fluxionality of the clusters—that is the dynamical changes in their structure(s) that can take place under the conditions of a given experiment. The latter implies continua of contributing configurations. Our analysis indicates that a representative "fingerprint" of these continua is furnished by select structures that correspond to *bona fide* barriers (transition states) and/or electronic-crossing configurations that may serve as effective barriers in electronically nonadiabatic dynamics. The special role of these barrier configurations as contributors to the measured spectra stems from their enhanced dynamical weighting that is a consequence of the slow-down of the dynamics at and in the vicinity of these configurations.

SUMMARY

In this communication, we presented and analyzed results of our combined experimental and computational study of anionic Al$_n$Pt$^-$, n = 1–7, clusters. Photoelectron spectroscopy measurements were performed to obtain their size-specific EBE spectra. The framework of the gradient-corrected DFT was used to identify and characterize computationally low-energy structural forms for each cluster size that included stable equilibrium conformations as well as transition state and electronic-crossing configurations. For each of these then, the spectrum of the EBEs was calculated using a post-DFT correction scheme we developed earlier.

The overall finding is that the structures we identified account remarkably well for the size-specific features and peculiarities of the measured spectra. The general message of the study is the importance of accounting for the possible contribution of multiple structural forms of a finite system into its measured PES spectrum. These forms include not only stable equilibrium conformations but also other configurations that are accessible under the condition of a given experiment.

An important further development in the field, which is partially already underway, is attaining the ability—both experimentally and computationally—to generate temperature-specific EBE spectra. Experimentally, the task is developing a better control over the temperature. Computationally, the challenge is to calculate accurately temperature-dependent free energies with entropic contributions that fully account for the anharmonicity of the studied system irrespective of its degree (*cf.*, *e.g.*, ref 25).

ASSOCIATED CONTENT

Supporting Information

The Supporting Information is available free of charge at https://pubs.acs.org/doi/10.1021/acs.jpca.2c03116.

https://doi.org/10.1021/acs.jpca.2c03116
J. Phys. Chem. A 2022, 126, 4241–4247

Results of test calculations; illustration of finding a TS using constrained optimizations on a grid of fixed interatomic distances; and illustration of finding an ECC using constrained optimizations on grids of fixed interatomic distances on two different electronic surfaces (PDF)

AUTHOR INFORMATION

Corresponding Authors

Paulo H. Acioli − *Department of Physics, Northeastern Illinois University, Chicago, Illinois 60625, United States;* orcid.org/0000-0001-5712-0183; Email: p-acioli@neiu.edu

Kit H. Bowen − *Departments of Chemistry and Materials Science, Johns Hopkins University, Baltimore, Maryland 21218, United States;* orcid.org/0000-0002-2858-6352; Email: kbowen@jhu.edu

Julius Jellinek − *Chemical Sciences and Engineering Division, Argonne National Laboratory, Lemont, Illinois 60349, United States;* orcid.org/0000-0001-8241-3623; Phone: (773) 477-9958; Email: jellinek@anl.gov

Author

Xinxing Zhang − *Collaborative Innovation Center of Chemical Sciences and Engineering, College of Chemistry, Nankai University, Tianjin 300071, China;* orcid.org/0000-0001-5884-2727

Complete contact information is available at: https://pubs.acs.org/10.1021/acs.jpca.2c03116

Notes

The authors declare no competing financial interest.

ACKNOWLEDGMENTS

The experimental part of this material is based upon work supported by the Air Force Office of Scientific Research (AFOSR) under grant number FA9550-19-1-0077 (K.H.B.). The theoretical work at Argonne was supported by the Office of Basic Energy Sciences, Division of Chemical Sciences, Geosciences and Biosciences, U.S. Department of Energy under contract no. DE-AC02-06CH11357 (J.J.) This research used in part the resources of the National Energy Research Scientific Computing Center (NERSC) supported by the Office of Science of the U.S. Department of Energy under contract no. DE-AC02-05CH11231.

REFERENCES

(1) Wang, L.-S. Photoelectron Spectroscopy of Size-Selected Boron Clusters: From Planar Structures to Borophenes and Borospherenes. *Int. Rev. Phys. Chem.* **2016**, *35*, 69−142.

(2) Lineberger, W. C. Once upon Anion: A Tale of Photodetachment. *Annu. Rev. Phys. Chem.* **2013**, *64*, 21−36.

(3) Jellinek, J.; Acioli, P. H. Computational Electron Spectroscopy of Gas Phase Metal Clusters. In *Atomic Clusters: From Gas Phase to Deposited*; The Chemical Physics of Solid Surfaces; Woodruff, D. P., Ed.; Elsevier: Amsterdam, 2007; Vol. *12*, pp 299−326.

(4) Acioli, P. H.; Zhang, X.; Bowen, K. H., Jr.; Jellinek, J. Electron Binding Energy Spectra of Al_nMo^- Clusters: Measurements, Calculations, and Theoretical Analysis. *J. Phys. Chem. C* **2019**, *123*, 7810−7817.

(5) Acioli, P. H.; Jellinek, J. Theoretical Analysis of Photoelectron Spectra of Pure and Mixed Metal Clusters: Disentangling Size, Structure and Composition Effects. *J. Phys. Chem. C* **2017**, *121*, 16665−16672.

(6) Acioli, P. H.; Jellinek, J. Electron Binding Energies of Anionic Magnesium Clusters and the Nonmetal-to-metal Transition. *Phys. Rev. Lett.* **2002**, *89*, 213402.

(7) Thomas, O. C.; Zheng, W.; Xu, S.; Bowen, K. H., Jr.; Shiloh, M. Onset of Metallic Behavior in Magnesium Clusters. *Phys. Rev. Lett.* **2002**, *89*, 213403.

(8) (a) Jellinek, J.; Acioli, P. H. Magnesium Clusters: Structural and Electronic Properties and the Size-Induced Nonmetal-to-metal Transition. *J. Phys. Chem. A* **2002**, *106*, 10919−10925. (b) Jellinek, J.; Acioli, P. H. Magnesium Clusters: Structural and Electronic Properties and the Size-Induced Nonmetal-to-metal Transition Erratum. *J. Phys. Chem. A* **2003**, *107*, 1670.

(9) Acioli, P. H.; Jellinek, J. Theoretical Determination of Electron Binding Energy Spectra of Anionic Magnesium Clusters. *Eur. Phys. J. D* **2003**, *24*, 27−32.

(10) Jellinek, J.; Acioli, P. H. *Computational Electron Spectroscopy—Application to Magnesium Clusters*; Lecture Series on Computer and Computational Sciences; Maroulis, G., Simos, T., Eds.; VSP: Leiden, 2005; Vol. *3*, pp 59−74.

(11) Jellinek, J.; Acioli, P. H.; Garcia-Rodeja, J.; Zheng, W.; Thomas, O. C.; Bowen, K. H., Jr. Mn_n^- Clusters: Size-Induced Transition to Half Metallicity. *Phys. Rev. B: Condens. Matter Mater. Phys.* **2006**, *74*, 153401.

(12) Li, X.; Grubisic, A.; Stokes, S. T.; Cordes, J.; Ganteför, G. F.; Bowen, K. H., Jr.; Kiran, B.; Willis, M.; Jena, P.; Burgert, R.; et al. Unexpected Stability of Al_4H_6: A Borane Analog? *Science* **2007**, *315*, 356−358.

(13) Zhang, X.; Wang, Y.; Wang, H.; Lim, A.; Gantefoer, G.; Bowen, K. H., Jr.; Reveles, J. U.; Khanna, S. N. On the Existence of Designer Magnetic Superatoms. *J. Am. Chem. Soc.* **2013**, *135*, 4856−4861.

(14) Ho, J.; Ervin, K. M.; Lineberger, W. C. Photoelectron Spectroscopy of Metal Cluster Anions: Cu_n^-, Ag_n^-, and Au_n^-. *J. Chem. Phys.* **1990**, *93*, 6987−7002.

(15) Becke, A. D. Density-functional Exchange-energy Approximation with Correct Asymptotic Behavior. *Phys. Rev. A: At., Mol., Opt. Phys.* **1988**, *38*, 3098−3100.

(16) Perdew, J. P. Density-Functional Approximation for the Correlation Energy of the Inhomogeneous Electron Gas. *Phys. Rev. B: Condens. Matter Mater. Phys.* **1986**, *33*, 8822−8824.

(17) Andrae, D.; Haeussermann, U.; Dolg, M.; Stoll, H.; Preuss, H. Energy-Adjusted *Ab Initio* Pseudopotentials for the Second and Third Row Transition Elements. *Theor. Chem. Acc.* **1990**, *77*, 123−141.

(18) Godbout, N.; Salahub, D. R.; Andzelm, J.; Wimmer, E. Optimization of Gaussian-type Basis Sets for Local Spin Density Functional Calculations. Part I. Boron through Neon, Optimization Technique and Validation. *Can. J. Chem.* **1992**, *70*, 560−571.

(19) Sosa, C.; Andzelm, J.; Elkin, B. C.; Wimmer, E.; Dobbs, K. D.; Dixon, D. A. A Local Density Functional Study of the Structure and Vibrational Frequencies of Molecular Transition-Metal Compounds. *J. Phys. Chem.* **1992**, *96*, 6630−6636.

(20) Frisch, M. J.; Trucks, G. W.; Schlegel, H. B.; Scuseria, G. E.; Robb, M. A.; Cheeseman, J. R.; Montgomery, J. A., Jr.; Vreven, T.; Kudin, K. N.; Burant, J. C.; et al. *Gaussian 03*, Revision C.02; Gaussian, Inc.: Wallingford CT, 2004.

(21) Jellinek, J.; Krissinel, E. B. Ni_nAl_m Alloy Clusters: Analysis of Structural Forms and their Energy Ordering. *Chem. Phys. Lett.* **1996**, *258*, 283−292.

(22) Jellinek, J.; Acioli, P. H. Converting Kohn-Sham Eigenenergies into Electron Binding Energies. *J. Chem. Phys.* **2003**, *118*, 7783−7796.

(23) Mercero, J. M.; Matxain, J. M.; Lopez, X.; York, D. M.; Largo, A.; Eriksson, L. A.; Ugalde, J. M. Theoretical Methods that Help Understanding the Structure and Reactivity of Gas Phase Ions. *Int. J. Mass Spectrom.* **2005**, *240*, 37−99.

(24) Zhang, X.; Ganteför, G.; Bowen, K. H., Jr.; Alexandrova, A. N. The $PtAl^-$ and $PtAl_2^-$ Anions: Theoretical and Photoelectron Spectroscopic Characterization. *J. Chem. Phys.* **2014**, *140*, 164316.

(25) Jellinek, J.; Aleinikava, D. Anharmonic Densities of States: A General Dynamics-based Solution. *J. Chem. Phys.* **2016**, *144*, 214103.